Research Article

Marek Woźniak*, Tomasz Szydłowski, and Krzysztof Siczek

The effect of dynamics of the swash plate–slippers–piston assembly on friction torques in bearings in compressor of cooling aggregate

https://doi.org/10.2478/mme-2020-0006
Received Dec 03, 2019; accepted Feb 07, 2020

Abstract: The swash plate type compressor utilized in car air conditioning devices and cooling system was analyzed in this study. Proper dynamic behavior of the components in such a compressor affected the correct functioning of the whole system. The aim of the study was to identify the characteristics of the main motion components in the swash plate–slippers–piston assembly of the compressor and to estimate the friction torques in its bearings. Some models of this assembly are elaborated and presented in the paper. The main components of slipper complex motion were identified, such as reciprocal motion along the axis of piston, rotation around piston axis, and short-time rotation around its own axis. Friction torque in axial bearing was higher than in journal bearing and varied with the rotational angle. Friction torques in journal bearings varied with the rotational angle and had different courses for two bearings of the compressor.

Keywords: compressor, bearing friction torque, swash plate–slipper–piston assembly, dynamics

1 Introduction

Air conditioning is a very important problem related to the comfort and safety during driving the cars, especially in conditions of elevated values of the ambient temperature and/or humidity. Nowadays, many vehicles with cold storages possessing a cooling system with the aggregate driven by the vehicle combustion engine via belt transmission can be met. The working cycle and varying loading and speed of the engine determine the cooling aggregate operation. Particularly, they determine the resistance to motion in the compressor bearings.

There are several types of compressors used in car air conditioning devices and cooling system.

According to [1], there are three types of compressors with fixed displacement, swash plate type, vane type, and scroll type, and one type with variable displacement, namely, one-way swash plate type. The swash plate type compressor is analyzed in this study. Compressor of such type is suitable for a wide range of vehicles. Proper dynamic behavior of components in such a compressor affects the correct functioning of the whole system. The aim of the study was to identify the characteristics of the main motion components in the swash plate–slippers–piston assembly of the compressor and to estimate the friction torques in its bearings.

According to [2], the compressor oil mixes with refrigerant during operation of a cooling aggregate and circulates inside the refrigeration system. The mixture of compressor oil and refrigerant can contain wear products originating as a result of cooperation of the sliding parts of the refrigeration compressor [3, 4]. Complex interactions in the oil–refrigerant mixture change the lubricating properties in comparison to the pure oil.

According to [5], studies on axial piston pumps mainly relate to forces between the elements in relative motion [6, 7], flow inside the pump [7], noise, and cavitation [8].

Latas and Stojek [9] elaborated a dynamic model of axial piston swash plate positive displacement pump. Lee and Lee [10] developed a simulation program for the performance analysis of variable displacement swash plate type compressor.

According to [11], in case of different motor speeds, the refrigerant compressor needs to adjust the displacement in order to control the cooling capacity. The adjustment is

***Corresponding Author: Marek Woźniak:** Department of Vehicles and Fundamentals of Machine Design, Lodz University of Technology, Stefanowskiego Str. 1/15, 90-537 Lodz, Poland
Tomasz Szydłowski, Krzysztof Siczek: Department of Vehicles and Fundamentals of Machine Design, Lodz University of Technology, Stefanowskiego Str. 1/15, 90-537 Lodz, Poland

reached by inclining the swash plate by angle α. The inclination itself is a function of the balance of forces. Besides the friction, inertia, and spring forces, the pressure difference between the crankcase and the cylinder capacity has the greatest influence and is controlled.

Tian *et al.* [12] developed the steady-state mathematical model of variable displacement swash plate compressor VDSC and verified it experimentally.

Zhang and Wang [13] reported that the coefficient of performance (COP) of the swash plate compressor with overflow channel was lower compared with the conventional compressor, but the volumetric efficiency and the cooling capacity of a swash plate compressor with overflow channel were better than those of a conventional compressor in terms of the same operation and dimension parameters.

According to [14], in axial piston pumps, the cylinder block and driveshaft are on the same centerline and the pistons reciprocate parallel to the drive shaft. The swash plate inline design is a simple type of such a pump. In these pumps, the size and number of pistons and also their stroke length determine the displacement. The stroke length is controlled by the swash plate angle. In variable displacement models, the swash plate is installed in a movable yoke. By pivoting the yoke on pintles, the swash plate angle and piston stroke can vary.

Zloto and Stryjewski [15] analyzed the load of the kinematic pair piston–cylinder block in an axial piston pump using spatial models of discrete and analog piston load.

Borghi *et al.* [16] analyzed variable displacement swash plate axial piston pumps. A lumped parameter model of the pump was elaborated, which allowed determination of the pressure transients within the pistons and then computation of instantaneous and average moments acting on the swash plate.

Kassem and Bahr [17] developed a mathematical model for the kinematics, piston chamber pressure, and output flow rate of swash plate axial piston pumps with conical cylinder blocks.

According to [18], the aircraft hydraulic pump is a variable displacement, pressure-compensated unit that adjusts the volume of fluid delivered to maintain constant pressure. In a hydraulic pump, the inclined angle of the swash plate affects the displaced volume. The discharge pressure controls the swash plate angle via the compensator valve and stroking piston.

According to [19], depending on the axial piston pump configurations, the angle of the load control actuator in the form of the swash plate or the bent-axis mechanism determines the effective stroke of the piston, and in effect, the torque output of the pump. A piston-type hydraulic pump with variable displacement can be modeled with a modified version of Wilson's P/M theory [20].

According to [21], varying both the volumetric displacement and the shaft speed of a variable displacement swash plate type piston pump allows minimization of power consumption in oil supply under constant pressure to a hydraulic cylinder controlled by valve, especially during idling. During classic operation, the pump speed was varied in a manner providing a constant system pressure, with a fixed maximum angle of the swash plate. At idling, the swash plate angle and pump speed were decreased to their minimum values.

Huang *et al.* [22] found that the combination of variable displacement and speed-variable pump drive was more efficient than a speed-variable pump drive or a variable displacement pump drive. The characteristics of pressure pulsations of a combination of variable displacement and speed-variable pump were investigated.

Srivastava *et al.* [23] elaborated a mathematical model for a double-acting fixed displacement swash plate compressor for evaluating the shaft torque and volumetric efficiency of the compressor. Such a shaft torque was a measure of the compressor power. The geometrical description of swash plate yielded a kinematic model to obtain the piston displacement as an explicit function of the angle of rotation of a shaft. A methodology was presented to evaluate in-cylinder gas pressures as a function of angle of rotation of a shaft. This kinematic model was extended to present a dynamic analysis of compressor, which yielded variation of torque with the rotation angle of the shaft. A method to model the volumetric efficiency was elaborated, which related the volumetric efficiency of the compressor to the rotational speed of the shaft.

2 Materials and Methods

2.1 Compressor of Cooling Aggregate

The studied aggregate was used in the Ford Focus vehicle with 2L SI engine manufactured in 2003. Analysis for the case of damage to the cooling aggregate in the vehicle with cold storage chamber was carried out [24]. The failure was initiated by damage of radial sealing ring, which appears to be harmless at first. However, it caused much more serious and complex consequences. When external impurities of high hardness, together with wear debris generated inside, got into the contact zone between mating surfaces, it resulted in blurring, hits, and plastic deformations of many elements. These phenomena resulted from the possi-

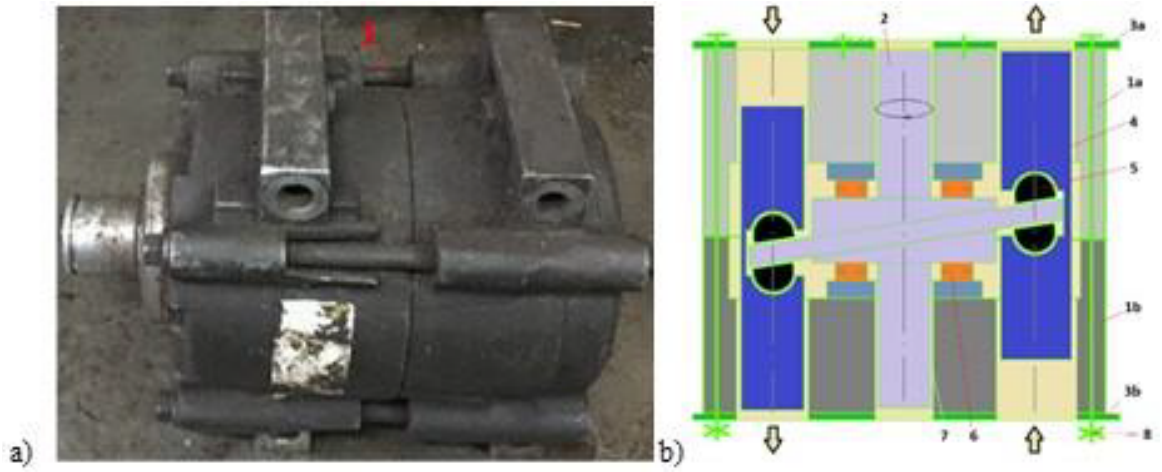

Figure 1: a) The axial five-piston pump of cooling aggregate compressor R57166. 1 – screw. b) Scheme of compressor. 1a, 1b – head components, 2 – shaft with the swash plate, 3a, 3b – valve plates, 4 – piston, 5 – slipper, 6 - needle roller bearing, 7 – sliding bearing, 8 – bolts

ble locking of pistons in cylinders under diluted oil and an occurrence of hard micrograins in contact zones. Finally, failure of the whole aggregate happened. Therefore, it was necessary to improve the relative positioning of the head components, that is, through additional pins. The material transfer between slippers and their seats was also identified.

The aggregate included the axial five-piston compressor R57166 (Figure 1a). The scheme of such a compressor is presented in Figure 1b. Relative to the head parts (1a and 1b) of the compressor, shaft (2) with swash plate was bearing axially using two needle roller bearings (6) and radially using two journal bearings (7). The swash plate mated with slippers (5). Two valve plates (3a and 3b) with both parts of the head were connected to the compressor housing through four steel bolts (8). Five aluminum alloy pistons (4) were led, via sealing rings made of rubber, in cylinders arranged in a radial pattern in the fixed aluminum alloy head parts (1a and 1b). One of them was fixed relative to the compressor housing (Figure 2), made of aluminum alloy, through two steel pins.

Figure 2 provides a better insight into the real components of the axial compressor. Pistons could make small radial and circumferential motions and swings within a clearance between the surfaces E1 and E2 and the surfaces F1 and F2. The pistons were driven through slippers made of steel, mating through their spherical surface B1 with spherical seat B2 made in pistons. Through their front surface A1, placed opposite to the spherical surface B1, the pistons were driven by the swash plate (surface A2) made of aluminum alloy. The swash plate was mounted on the rotating steel shaft via splined connection. The shaft journals (surface C1) could also make small radial motions and swings within a clearance in the bronze journal bearings (surface C2). The swash plate (surface D2) could make small motions within an axial clearance occurring in two axial needle roller bearings (surface D1).

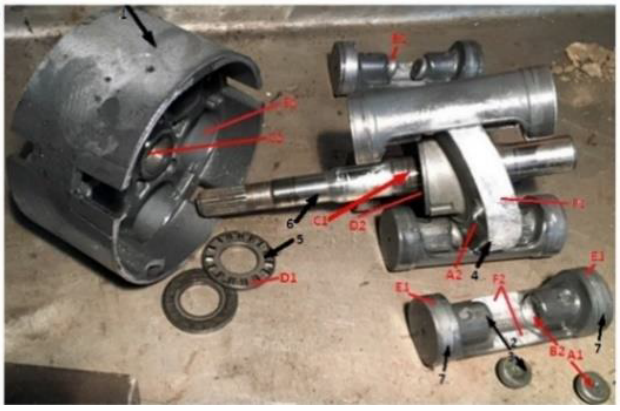

Figure 2: Components of the axial compressor of cooling aggregate. 1 – head component, 2 – piston, 3 – slipper, 4 - the swash plate, 5 - needle roller bearing, 6 – rotating shaft, 7 – sealing rings

2.2 The simulation model for motion of the swash plate–slippers–piston assemblies

The motion of elements in five swash plate–slippers–piston assemblies in the compressor is very similar; however, it is delayed in time according to the operating cycle of the axial piston compressor. The nature of motion components for elements in each mentioned assembly is diffi-

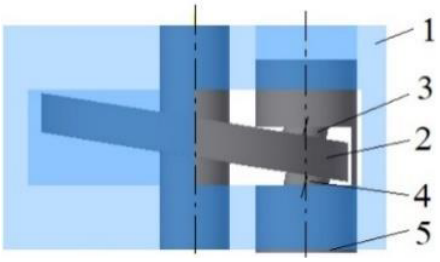

Figure 3: Simplified model of the single compressor section. 1 – body with cylinder, 2 – shaft with swash plate, 3, 4 – slippers, 5 – piston

cult to predict due to complexity of such motion. To identify the main motion components, the multibody model of the single swash plate–slippers–piston assembly was elaborated. The model components were rigid solid bodies connected to each other through nonlinear joints. The parameters of such joints were evaluated based on experiment and a review of literature. To simplify analysis, it was assumed that:

- the shaft is coaxial with its journal bearing and can only make rotation around its axis;
- the piston is coaxial with the cylinders in the head parts of the compressor and the axis of cylinder is parallel to the axis of shaft;
- the piston can make a reciprocal motion along the axis of cylinder;
- the centers of spherical slipper seats made in the piston lay on the piston axis;
- the plane surface of slipper is always tangent to the plane of the swash plate and the distance between such planes is constant; and
- the slipper can rotate around the center of its spherical seat made in the piston.

2.3 The squeezing between slipper and swash plate

According to [25], the lubricant flow via the slipper/swash plate gap includes Poiseuille, Couette, and squeeze flows. The Poiseuille one is affected by the differential pressure between the slipper chamber and the pump case; the Couette flow depends on the velocity of revolution motion and one of slipper spin motion; the squeeze flow is related to the squeeze velocity of the slipper.

A very small value of the oil film depth causes a very small variation of pressure in the direction of oil film depth which can be neglected.

The pressure distribution of oil film in the slipper–swash plate contact zone can only be a function of the variable r.

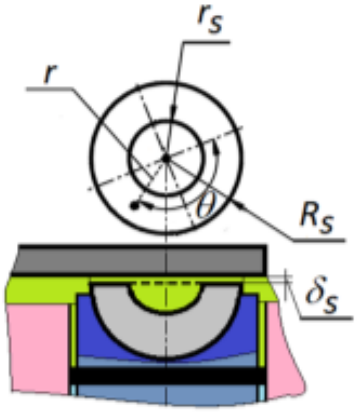

Figure 4: Diagram for the derivation of lubricant layer between slipper and swash plate.

According to [25], pressure in the gap between slipper and swash plate can be obtained from Equation (1):

$$p = (p_s - p_d)\frac{\ln(r_s/r)}{\ln(R_s/r_s)} + \frac{3\mu}{\delta_S^3}\frac{d\delta_S}{dt}\left[\left(r^2 - r_S^2\right) - \left(r_S^2 - R_S^2\right)\frac{\ln(r_s/r)}{\ln(R_s/r_s)}\right] + p_S \quad (1)$$

The leakage flowing from the slipper chamber to the pump case is described by the left side of Equation (2). The first term on the left of Equation (24) represents the leakage flow caused by the differential pressure effect and the second and third terms represent the leakage flow caused by the squeeze effect.

$$\left[\frac{\pi}{2}\frac{\left(R_S^2 - r_S^2\right)}{\ln\left(R_S/r_S\right)} - \pi r_S 2\right]\frac{d\delta_S}{dt} + \frac{\pi\delta_S^3}{6\mu}\frac{p_S - p_d}{\ln\left(R_S/r_S\right)} = \frac{\pi R_S^2\delta_S}{K_e}\frac{dp}{dt} \quad (2)$$

The right side of Equation (24) describes the effect of fluid compressibility of oil in the slipper chamber. Equations (23) and (24) with the boundary condition that $p = p_d$ for $r = R_s$ allowed obtaining lubricant layer thickness δ_s.

2.4 The squeezing between swash plate and slipper

It was assumed that the space between the socket and slipper spherical surfaces is filled with a lubricant. It was also assumed that the slipper does not rotate significantly

about its center; rather, the slipper moves along some path inside the socket boundaries. In a spherical joint, the squeeze film action is dominant when the relative rotational velocity between the ball and the socket is small compared to the relative radial velocity. In the present study, the squeeze film effect is the only lubrication action considered. This phenomenon results from the two approaching spherical surfaces as the lubricant experiences normal pressure. According to [26], to evaluate the lubrication forces developed in a spherical joint with lubricant, the pressure flow is equated to the pressure that results from displacement associated with the geometric configuration of the spherical joint elements. The configuration considered here is of a hemispherical seat which, owing to symmetry, has a cross section shown in Figure 5.

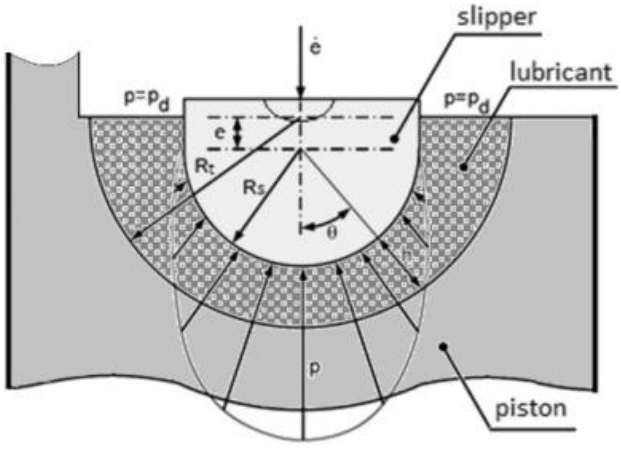

Figure 5: Generic representation of a spherical lubricated joint with squeeze film.

According to [27], for a spherical joint with lubricant, the amount of fluid that passes a conical element surface is given by Equation (3):

$$Q = -\frac{\pi R_i \sin\theta h^3}{6\mu R_i}\frac{dp}{d\theta} \tag{3}$$

where R_i is the ball radius, h represents the thickness of the film lubricant, μ is the dynamic lubricant viscosity, θ is the angular coordinate, and p is the pressure. The negative sign of Equation (3) reflects the fact that the fluid flows down the pressure gradient. In addition, from the geometry of a spherical joint, the fluid film thickness can be expressed as follows [27]:

$$h = c\,(1 - \epsilon\cos\theta) \tag{4}$$

in which the eccentricity ratio, ϵ, is given by Equation (5) [27]:

$$\epsilon = e/c \tag{5}$$

with e and c being the magnitudes of the eccentricity and radial clearance, respectively.

On the other hand, the flow due to the radial velocity, $\dot{e}$, is expressed as [27]:

$$Q = \pi\dot{e}R_i^2 sin^2\theta \tag{6}$$

where $\dot{e}$ is the velocity of the ball center that is responsible for the squeeze film action, that is, $\dot{e} = \frac{dh}{dt}$. This parameter can be evaluated by differentiating Equation (4) with respect to time. Equation (6) corresponds to the total flow rate through the spherical joint, and hence, it represents the amount of fluid that flows through the joint and is required to ensure a desired fluid thickness equal to h.

Thus, for the flow continuity, combining Equations (3)–(6) results in the general expression for pressure gradient dp as follows [27]:

$$dp = \frac{6\mu\dot{e}\sin\theta}{(c/R_i)^3 R_i(1-\epsilon\cos\theta)^3}d\theta \tag{7}$$

According to [27], the boundary conditions of the lubricant flow in the present study are given by Equation (8):

$$p\left(\pm\pi/2\right) = p_d \tag{8}$$

Thus, the pressure distribution is obtained by integrating Equation (7) with the boundary conditions of Equation (8), yielding

$$p = p_d + \frac{3\mu\dot{e}}{(c/R_i)^3 R_i\epsilon}\left[1 - \frac{1}{(1-\epsilon\cos\theta)^2}\right] \tag{9}$$

Finally, the resulting squeeze F_S film force on the ball, which is applied to equilibrate the fluid pressure, can be evaluated as the integral of the pressure field over a hemisphere, that is,

$$F_S = 2\pi R_i^2 \int_0^{\pi/2} p\sin\theta\cos\theta d\theta \tag{10}$$

from which

$$F_S = \frac{p_d}{2} - \frac{6\pi\mu\dot{e}R_i}{(c/R_i)^3}\left[\frac{1}{\epsilon^3}ln\,(1-\epsilon) + \frac{1}{\epsilon^2\,(1-\epsilon)} - \frac{1}{2\epsilon}\right] \tag{11}$$

Is obtained.

2.5 The loading of contact zone between slipper and swash plate

The scheme of loading the single swash plate–slippers–piston–cylinder assembly is shown in Figure 6. It was assumed in the model that all the components are rigid. Contact zones between the swash plate and slippers and the

slippers and their hemispherical seats in the piston were filled with lubricant. To simplify the analysis of normal forces in the contact zones, the changes in lubricant layer thickness were omitted. The frictional forces in such contact zones that acted on the piston were also omitted as ones of small values. The contact pressure in the zones between the rubber sealing rings and the cylinder was assumed to be uniform, as the length L_S of the sealing ring was small in comparison with the piston length $2L + L_H$ (Figure 6). During the rotation of shaft with swash plate, reciprocal motion of the piston relative to the cylinder occurred due to the shaping effect of the swash plate via sippers on the piston. The displacement x, velocity v, and acceleration of piston during its reciprocal motion relative to the cylinder are given by Equations (12)–(14):

$$x = Rtg\gamma\,(1 - \cos\varphi) \tag{12}$$

$$v = \frac{dx}{dt} = R\omega tg\gamma \sin\varphi \tag{13}$$

$$a = \frac{d^2x}{dt^2} = R\omega^2 tg\gamma \cos\varphi \tag{14}$$

where R is the radius of circle of the cylinder surface including the cylinder axes, γ the tilted angle, ϕ the rotation angle, and ω is the angular speed of the shaft with swash plate.

The balance of forces acting on the piston parallel to its axis is described by Equation (15):

$$m_p a = \frac{\pi}{4}d^2 p_{s1} - N\cos\gamma - f(F_a + F_b) - Bv - \frac{\pi}{4}d^2 p_{s2} - \frac{\pi}{4}\left(d^2 - k^2\right)p_d + \frac{\pi}{4}d^2 p_d \tag{15}$$

where p_{s1} and p_{s2} are the pressure at the sides of piston, p_d is the pressure inside the compressor, m_p the piston weight, f the kinematic friction coefficient in contact rubber sealing ring–cylinder, B the viscous damping coefficient caused by oil in the gap between piston and cylinder, d the diameter of piston, r_t the radius of spherical seat in the piston, and k is the diameter of the seat in the piston in the planes normal to the piston axis and distant from each other by the length L_H.

The balance of forces acting on the piston normal to its axis is described by Equation (16):

$$F_a + F_b - N\sin\gamma = 0 \tag{16}$$

The balance of moments acting on the piston is described by Equation (17):

$$-F_a\,(0.5L_H + L - 0.5L_S) + F_b\,(0.5L_H + L - 0.5L_S) - N\sin\gamma\,(0.5L_H + r) = 0 \tag{17}$$

The forces F_a and F_b acting on the rubber sealing rings are given by Equations (18) and (19):

$$F_a = N\sin\gamma\frac{L - r - \frac{L_S}{2}}{2L + L_H - L_S} \tag{18}$$

$$F_b = N\sin\gamma\frac{L + L_H + r - \frac{L_S}{2}}{2L + L_H - L_S} \tag{19}$$

The normal force N loading the contact zones between the swash plate and slippers is given by Equation (20):

$$N = \frac{\frac{\pi}{4}d^2\,(p_{S1} - p_{S2}) + \frac{\pi}{4}k^2 p_d - m_p R\omega^2 tg\gamma\cos\varphi}{\cos\gamma + f\sin\gamma} - \frac{BR\omega tg\sin\varphi}{\cos\gamma + f\sin\gamma} \tag{20}$$

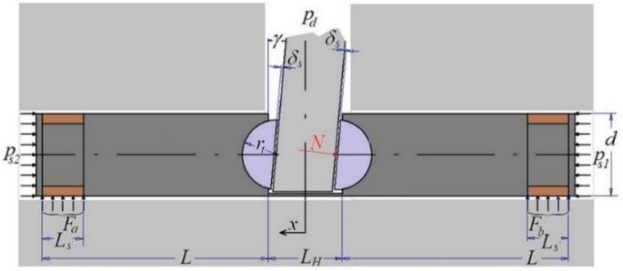

Figure 6: Scheme of loading the swash plate–slippers–piston–cylinder assembly.

The assumed course of pressure p in one side of the compressor cylinder as a function of time t is shown in Figure 7.

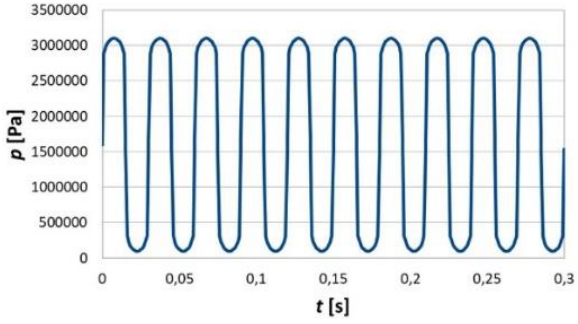

Figure 7: The assumed course of pressure p in one side of the compressor cylinder versus time t.

2.6 Rotation of slipper around its axis

The rotation of slipper around its axis is forced by friction torque acting in the contact zone between the slipper and

the swash plate. Such motion is resisted by the inertia of slipper and the friction torque in the contact zone between the slipper and its semi-spherical seat in the piston.

The model of lubricant layer in the contact zones, slipper–piston and slipper–swash plate, during slipper rotation around its axis is presented in Figure 8. It was assumed, for simplicity of analysis, that the slipper flat face was parallel to the plane of swash plate and the distance between them was equal to s_0. Maximal braking friction torque in the contact zone between the slipper and its seat in the piston occurred when the thickness s of the lubricant layer was equal to zero therein.

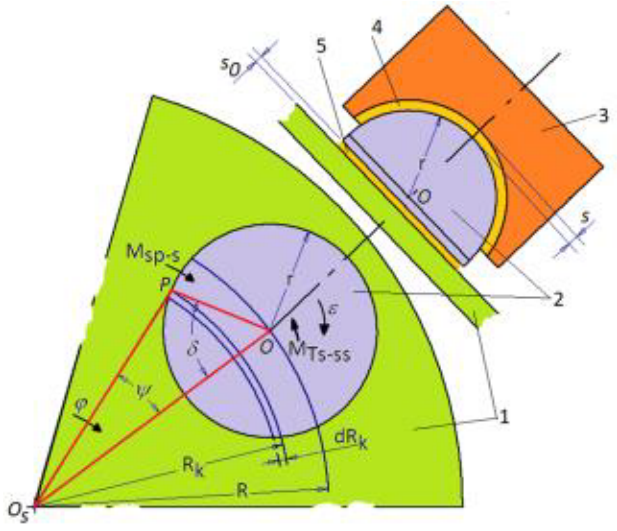

Figure 8: Model of lubricant layer in the contact zones, slipper–piston and slipper–swash plate, during slipper rotation around its axis. 1 – swash plate, 2 – slipper, 3 – piston, 4 – lubricant layer in contact slipper–piston spherical seat, 5 – lubricant layer in contact slipper–swash plate

Equation (21) describes the slipper rotation dynamics:

$$M_{sp-s} = M_{Ts-ss} + I \cdot \ddot{\epsilon} \tag{21}$$

The friction torque between the slipper and swash plate is given by Equations (22) and (23):

$$\begin{aligned} dM_{sp-s} &= R_k(\theta) \cdot dT = R_k(\theta) \cdot \mu_{sp-s} \cdot p \cdot dT \\ &= R_k(\theta) \cdot \mu_{sp-s} \cdot p \cdot R_k(\theta) \cdot \psi \cdot dR_k \\ &= \sqrt{\left(R^2(\theta) + r^2 - 2 \cdot R(\theta) \cdot r \cdot \cos\delta\right)} \\ &\cdot \mu_{sp-s} \cdot p \cdot R(\theta) \cdot r \\ &\cdot \sin^{-1}\left(\frac{r \cdot \sin\delta}{\left(R^2(\theta) + r^2 - 2 \cdot R(\theta) \cdot r \cdot \cos\delta\right)}\right) \\ &\cdot \sin\delta \cdot d\delta \end{aligned} \tag{22}$$

$$M_{sp-s} = 2 \cdot \int_0^{\pi} dM_{sp-s} \tag{23}$$

Assuming that the pressure distribution in the contact zone between slipper and swash plate is constant, the average value of such contact pressure was estimated from Equation (24):

$$p = \frac{N}{\pi \cdot R_s^2} \tag{24}$$

Assuming constant pressure distribution in the contact zone between slipper and its seat in the piston, the friction torque between the slipper and piston was estimated from Equation (25):

$$M_{Ts-ss} = \mu_{s-ss} \cdot N \cdot \frac{2}{3} \cdot R_s \tag{25}$$

Time of slipper rotation around its axis was estimated from Equation (26):

$$t = \frac{s}{\frac{v}{2}} = \frac{2 \cdot s}{\omega \cdot Raver(\theta) \cdot \tan\gamma} \tag{26}$$

Radius $R(\theta)$ changes during shaft rotation; but due to simplicity of calculation, its average value given by Equation (27) was used:

$$\begin{aligned} R_{aver}(\theta) &= 0.5 \cdot \left[R_{max}(\theta) + R_{min}(\theta)\right] \\ &= 0.5 \cdot \left(\frac{R}{\cos\gamma} + R\right) \end{aligned} \tag{27}$$

Resulting angle of slipper rotation around its axis related to the estimated time of such rotation t was estimated from Equation (28):

$$\epsilon = \ddot{\epsilon} \cdot \frac{t^2}{2} = \frac{M_{sp-s} - M_{Ts-ss}}{I} \cdot \frac{t^2}{2} \tag{28}$$

2.7 Rotation of slipper around the piston axis

The rotation of slipper around the piston axis is forced by shaped impact of the rotating swash plate on the slipper. If the slipper is in contact with the swash plate and the piston set, the rotational motion can be braked by friction torque M_{s-ss} generated in the contact zone between slipper and its semi-spherical seat in the piston. This condition can lead to slipper rotation around the piston axis with a constant rotational speed or to deceleration of such motion. Slipper rotation around the piston axis is described by Equation (29):

$$M_{sT} - M_{s-ss} = I \cdot \ddot{\epsilon} \tag{29}$$

Rotation of slipper around the piston axis resulted in generation of parallel and equal, but opposite reactions in

the contact zones swash plate–slipper and slipper–piston seat, respectively. They were spaced apart by the distance r_t. The shaped impact of swash plate on the slipper was considered to be equivalent to the gyroscopic torque M_{sT} affecting the slipper and is given by Equation (30):

$$M_{sT} \approx N \cdot \tan(\gamma) \cdot r_t = 0.5 \cdot (I_1 - I_2) \cdot \omega^2 \cdot sin^2(2\gamma) \quad (30)$$

The friction torque M_{s-ss} in the contact zone between slipper and its seat in the piston is given by Equation (31). It was assumed that the pressure distribution in the contact zone between slipper and its seat in piston is constant.

$$M_{s-ss} = N \cdot \cos\gamma \cdot \mu_{s-ss} \cdot \frac{2}{3} \cdot R_s \quad (31)$$

When the slipper is not in contact with its seat in the piston, accelerated slipper rotation around the piston axis can take place. Such acceleration is mainly caused by the squeezing torque $M_{squeeze}$ in the gap filled with lubricant and existing between swash plate and plane slipper face skewed to each other with the tilted angle α (Figure 9).

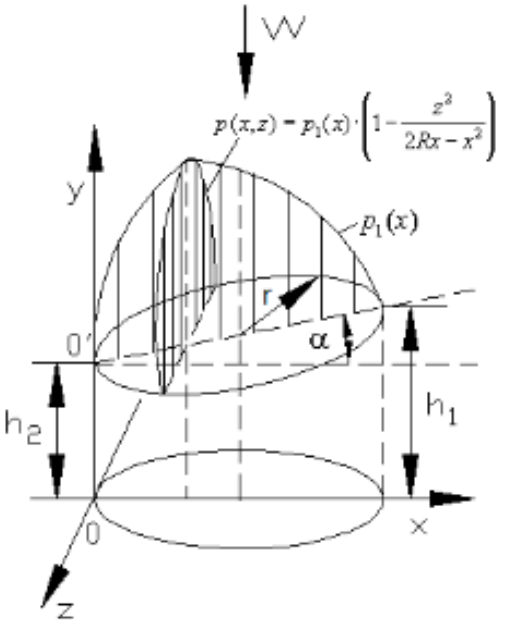

Figure 9: Geometry of the interstice between slipper and swash plate [28].

During acceleration, the slipper rotation around the piston axis is given by Equation (32):

$$M_{squeeze} \approx F(\alpha) \cdot \frac{4}{3} \cdot r = I_2 \cdot \ddot{\varepsilon} \quad (32)$$

Integrating the pressure distribution in the slipper–swash plate contact zone, using Equation (33), allows obtaining the force $F(\alpha)$. The pressure distribution shown in Figure 9 is described by Equation (34) [28]:

$$F(\alpha) = \iint_S p(x,z)\, dxdz \quad (33)$$

$$p(x,z) = \frac{6\eta w}{(\tan\alpha)^2} \left[\frac{1}{h(x)} - \frac{h_1 h_2}{h(x)^2 (h_1 + h_2)} - \frac{1}{h_1 + h_2}\right] \left(1 - \frac{z^2}{2Rx - x^2}\right) \quad (34)$$

where h is the film thickness, h_1 the maximum film thickness, h_2 the minimum film thickness, R the radius, w the squeezing velocity, and η is the lubricant dynamic viscosity.

The nondimensional load capacity $\overline{F}$ versus tilted angle α can be estimated (by fitting polynomial formula) from the course presented in the Figure 10 [28].

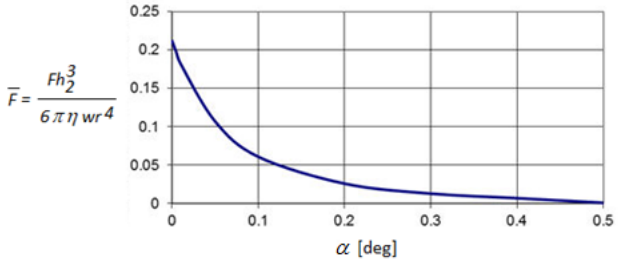

Figure 10: The nondimensional load capacity $\overline{F}$ versus tilted angle α [28].

2.8 Friction torque in journal bearing

The friction force FT in the radial journal bearing was calculated under the assumption that clearance of bearing was filled with lubricating oil. It is given by Equation (35). This is true for both surfaces of shaft and bearing hole. The planar cross section of the journal bearing is presented in Figure 11.

$$F_T = \frac{c\varepsilon W}{2R} \sin\psi + \frac{2\pi\eta \mathrm{URL}}{c\left(1 - \varepsilon^2\right)^{1/2}} \quad (35)$$

The first-term results are from the offset between the center of the shaft and that of the bearing. The second represents the Newtonian friction.

The resultant force W loading bearing contains two components, W_x and W_y, resulting from a double integration of the pressure varying both in the θ and y directions. W_x is the component along the line of centers and W_y is the one normal to it.

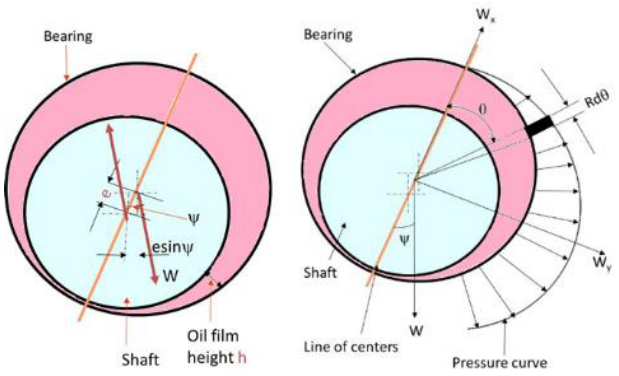

Figure 11: The planar cross section of the journal bearing.

The resultant load was obtained from Equation (36):

$$W = \sqrt{W_x^2 + W_y^2} = \frac{U\eta L^3}{c^2}\sqrt{\left[\frac{\pi^2\epsilon^2}{16\left(1-\epsilon^2\right)} + \frac{\epsilon^4}{\left(1-\epsilon^2\right)^4}\right]} \tag{36}$$

The attitude angle was given by Equation (37):

$$\tan\psi = \frac{W_y}{W_x} = \frac{\pi}{4}\cdot\frac{\left(1-\epsilon^2\right)^{1/2}}{\epsilon} \tag{37}$$

According to [29], the load capacity of sliding journal bearing can be estimated from Equations (38) to (49):

$$\overline{W} = \frac{c^2}{\omega\eta D^4}W \tag{38}$$

$$Y = log\left(\overline{W}\right) \tag{39}$$

$$X = log\left(L/D\right) \tag{40}$$

$$Y = C_3X^3 + C_2X^2 + C_1X + C_0 \tag{41}$$

$$C_3 = \frac{2\left[f_S(\epsilon) - f_L(\epsilon) + X_L + X_S\right]}{\left(X_L - X_S\right)^3} \tag{42}$$

$$C_2 = \frac{2 - 3C_3\left(X_L^2 - X_S^2\right)}{2\left(X_L - X_S\right)} \tag{43}$$

$$C_1 = -3C_1X_S^2 - 2C_2X_S + 3 \tag{44}$$

$$C_0 = -3C_3X_L^3 - C_2X_L^2 + \left(1 - C_1\right)X_L + f_L(\epsilon) \tag{45}$$

$$f_S(\epsilon) = log\left\{\left[1.0 - 0.7(\epsilon - 0.1)^{10}\right] \cdot \frac{\pi\epsilon\left(0.62\epsilon^2 + 1\right)^{1/2}}{8\left(1-\epsilon^2\right)^2}\right\} \tag{46}$$

$$f_L(\epsilon) = log\left\{(0.91 + 0.19\epsilon) \cdot \frac{3\epsilon\left(4\epsilon^2 + \pi^2 - \pi^2\epsilon^2\right)^{1/2}}{4\left(2+\epsilon^2\right)\left(1-\epsilon^2\right)}\right\} \tag{47}$$

$$X_S = log\left(1/8\right) \tag{48}$$

$$X_L = log\left(4.75\right) \tag{49}$$

The solution for such a set of equations is applicable for: $1/8 \le L/D \le 2$and $0 < \epsilon \le 0.9$.

For the longer journal bearing, Equations (38)–(49) were used, and for the shorter one, Equations (35) and (36) were used.

The friction torque was obtained from Equation (50):

$$M_T = F_T \cdot r_s \tag{50}$$

where r_s is the radius of shaft journal.

2.9 Friction torque in axial needle roller bearing

The coefficient of friction in rolling bearings relates to the type of bearing, the speed of rotation, the load, the amount and viscosity of the lubrication, the friction of the seals, etc. The bearing friction torque M_R (Nmm) can be estimated from Equation (51) [30, 31]:

$$M_R = M_0 + M_1 \tag{51}$$

Friction torque M_0 (Nmm) as a function of speed is given by Equation (52) [30, 31]

$$M_0 = f_0 \cdot (\nu \cdot n)^{2/3} \cdot d_M^3 \cdot 10^{-7} \tag{52}$$

for $(\nu \cdot n) \ge 2000$ and by Equation (53) [29, 30]

$$M_0 = f_0 \cdot 160 \cdot d_M^3 \cdot 10^{-7} \tag{53}$$

for $(\nu \cdot n) < 2000$.

Friction torque M_1 (Nmm) as a function of load is calculated from Equation (54) [30, 31]

$$M_1 = f_1 \cdot P_1 \cdot d_M \tag{54}$$

where P_1 (N) is the axial load for axial bearing, n (rpm) the operating speed, ν (mm^2/s) the kinematic viscosity of lubricant at the operating temperature, d_M (mm) the mean

diameter of bearing calculated from the formula $d_M = 0.5 \cdot (d + D)$, d (mm) = diameter of the bore of the bearing (shaft diameter)(mm), and D (mm) = outside diameter of the bearing (mm).

For axial roller bearing, f_0 = 3–4 and f_1 = 0.0015 [30, 31].

2.10 Reactions in axial and journal bearings

Reactions in axial rolling bearing and slide journal bearing were obtained using the model (Figure 12) containing the shaft with the swash plate 1, two journal-bearing bushes 2 and 3, two axial bearings containing housing washer 4, cage with rolling components 5, and shaft washer 6 treated as elastic solids made of materials as in real. On the opposite sides of the swash plate 1 were made very shallow holes 1A and 1B that were cylindrical deepening of the contact marks between the swash plate and slippers. Their placement could be rearranged relative to the position of the groove made in the shaft and taking into account the current rotation angle of the shaft 1. Such rearrangements were necessary as the positions of cylinders relative to the swash plate varied at the same time. Analysis was made assuming quasi-static loading of the shaft for a given rotational speed of the shaft.

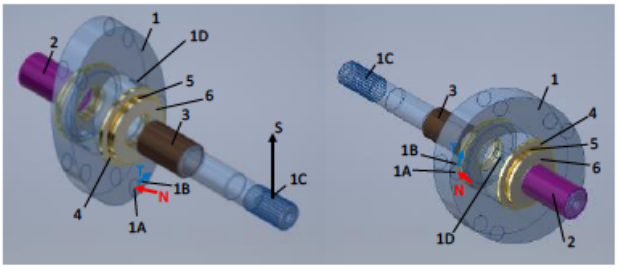

Figure 12: Model of the shaft with the swash plate 1, two journal-bearing bushes 2 and 3, two axial bearings containing housing washer 4, cage with rolling components 5, shaft washer 6.

The boundary conditions in the model were the following:

- Only axial displacements of housing washer 4 were allowed and journal-bearing bushes 2 and 3 were fixed.
- On the frontal surfaces of housing washer 4 were introduced force with values equal to 0 or 1 necessary to induce minimal axial bearing load.
- On the frontal surface 1A of the shallow holes were introduced values of contact pressure between the swash plate and slippers for a given moment. They are given by Equation (55):

$$p_{sp-s} = \frac{N}{2\pi r_t} \tag{55}$$

where N is the force between the slipper and the swash plate calculated from Equation (20) – for one side of the swash plate, only values in accordance to the sign of vector normal to the outer plane of swash plate were used respectively, and if such values were opposite, they were assumed to be equal to 0 and r_t is the radius of spherical seat in the piston.

- On the cylindrical surface of the shallow hole 1B were introduced friction force between the swash plate and the slipper tangential to the swash plate surface and acting in a peripheral direction of the shaft equal to the force of friction calculated from Equation (56):

$$T = \mu_{sp-s} \cdot N \tag{56}$$

- On the cylindrical surface 1C of the spline, a vertical force S equal to the force of the belt drive driving the shaft was introduced.

The mesh of finite elements was created automatically by the program Autodesc Inventor (Figure 13). Between the components were introduced contact elements allowing sliding.

Figure 13: Mesh of finite elements in the model.

The model allowed obtaining contact pressure in the contact zones between the shaft and the journal-bearing bushes and between rollers and washers.

The axial and radial reactions were calculated using Equation (57)

$$R = \sum_{i=1}^{i=n_e} p_{ci} \cdot A_{ei} \tag{57}$$

where p_{ci} is the contact pressure for the ith contact finite element, $A_{ei}$the area of the ith contact finite element, and n_e is the number of contact finite elements for the given contact zone.

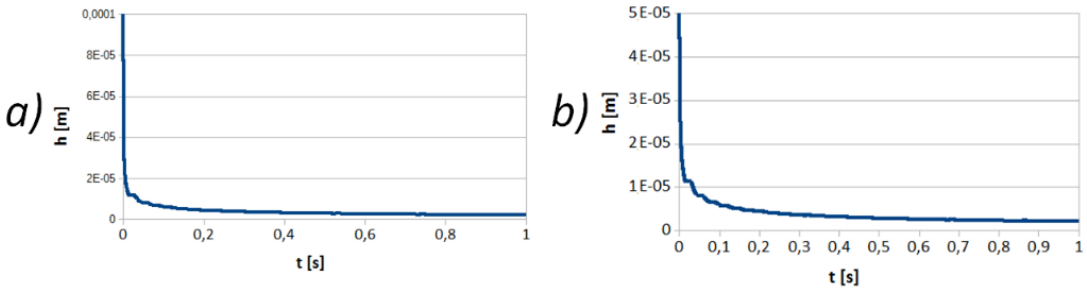

Figure 14: The thickness $h = \delta_s(t)$ of lubricant in the contact zone between slipper and swash plate against time t for initial value of $h = \delta_{s0}(t)$: a) $h = \delta_{s0}(t) = 0.05$ mm, b) $h = \delta_{s0}(t) = 0.1$ mm.

3 Results

The thickness $h = d_s(t)$(t) of the lubricant layer in the contact zone between slipper and swash plate against time t for different initial values of $\delta_{s0}(t)$ is shown in Figure 14. It is clearly seen that during the reciprocal motion of slipper along the piston axis, the thickness of lubricant in the slipper–swash plate contact zone quickly decreases and stabilizes.

The obtained values of the force N between the slipper and the swash plate as a function of time t are presented in Figure 15. Such values are lower than 1000 N. Values of the displacement x against time t for points laying on the cylinder axis and belonging to the plane surface of upper slipper, upper surface of swash plate, bottom surface of swash plate, and the plane surface of bottom slipper, respectively, are shown in Figure 16. The corresponding phase diagram (speed v against displacement x) for points laying on the piston axis and belonging to the plane surface of upper slipper and the plane surface of bottom slipper is presented in Figure 16b. Although the phase diagrams are similar, they are different from each other during short time periods when changes of contact zones between the swash plate and the opposite slippers occur within the clearance between them.

The calculated values of time t and rotation angle ϵ of the slipper against its own axis for two different rotational speeds of the compressor shaft are shown in Table 1. It is clearly seen that increasing the rotational speed of the shaft with swash plate by 30% causes a decrease of rotation time (by 25%) and angle (by 46%) of the slipper around its axis.

The course of angular speed ω of the slipper against time t during rotation of the slipper around the piston axis is shown in Figure 17. The narrow changes of angular speed take place during changes of contact zones between the swash plate and the opposite slippers, within the clearance between them.

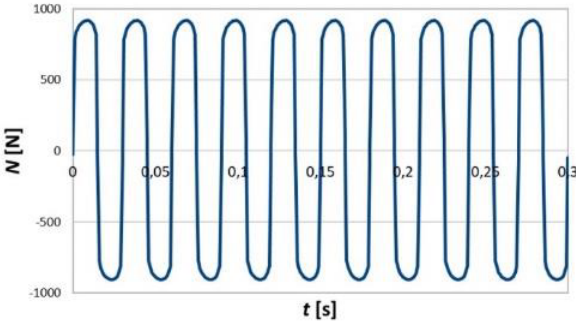

Figure 15: The course of the force N between the slipper and the swash plate of the axial compressor against time t.

Table 1: Time t and rotation angle ϵ of the slipper against its own axis for different rotational speeds of the compressor shaft

n (rpm)	2000	1500
t (s)	0.00018	0.00024
ϵ (rad)	1.073	1.855

Examples of contact pressure gradients in journal-bearing bushes and in the rolling components of axial bearings are shown in Figure 18. The right-side picture is shown in a different scale to emphasize contact pressure in journal-bearing bushes. The resulting contact pressure in the contact zones between the shaft journals and their bearing bushes can reach 20 MPa. The phenomenon of their concentration at the bearing edges can occur. The contact pressure between the rolling elements and their washers can reach maximal values of 175 MPa and average values of 80 MPa.

The resulting values of friction torque in journal bearings A and B against the rotation angle of compressor shaft with the swash plate is shown in Figure 19. It is clearly seen that the friction torques in the two journal bearings of compressor vary with the rotational angle and are not similar.

The friction torque values in axial needle bearing against the rotation angle of shaft with swash plate are pre-

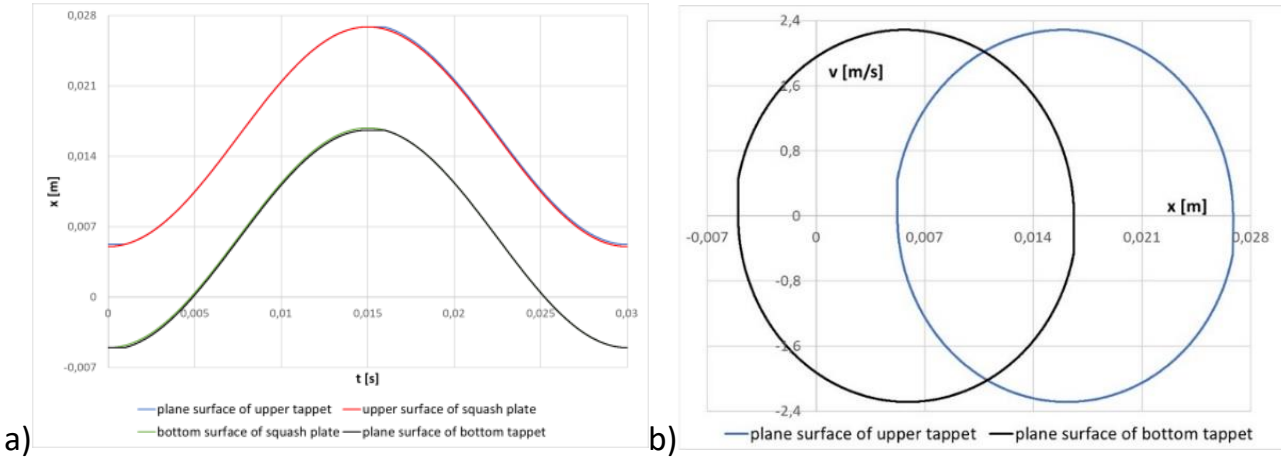

Figure 16: a) Course of displacement x against time t for points laying on cylinder axis and belonging to the plane surface of upper slipper, upper surface of swash plate, bottom surface of swash plate, and the plane surface of bottom slipper, respectively. b) Phase diagram (speed v against displacement x) for points laying on the piston axis and belonging to the plane surface of upper slipper and the plane surface of bottom slipper, respectively.

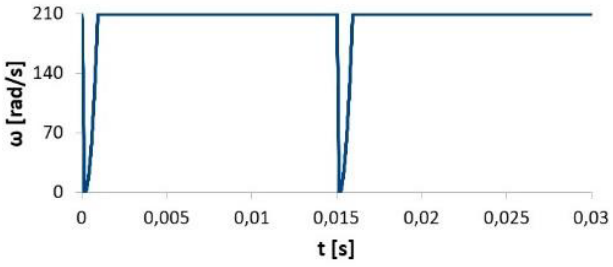

Figure 17: Course of angular speed ω of the slipper against time t during slipper rotation around the piston axis.

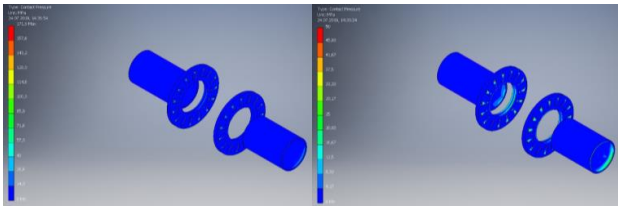

Figure 18: The contact pressure gradients in journal-bearing bushes and in the rolling components of axial bearings. The figure on right shows the contact pressure values in a higher scale.

sented in Figure 20 for the initial tension force $F_a = 0$ N and $F_a = 100$ N. For the last case, the obtained values of the friction torque in axial bearing are about 10% higher than in cases without the initial tension force F_a.

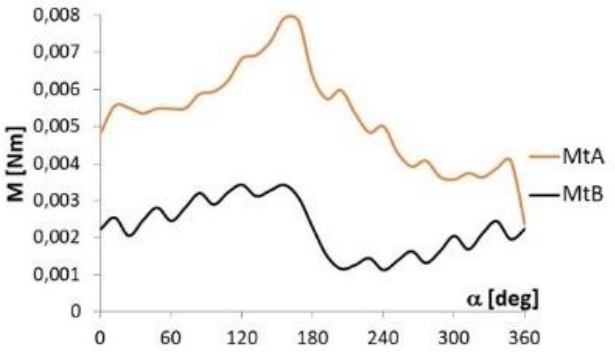

Figure 19: Friction torque in journal bearings A and B against the rotation angle of compressor shaft.

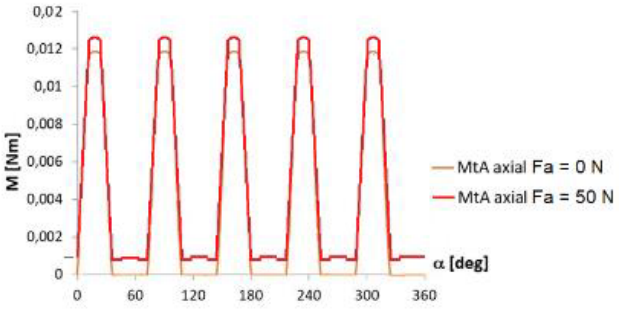

Figure 20: Friction torque in axial needle bearing against the rotation angle of shaft with swash plate.

4 Summary

The analysis carried out showed that motion of the slipper is very complex. The main components of it are: reciprocal motion along the axis of piston, rotation around piston axis, and short-time rotation around its own axis. The increase of rotational speed of the shaft with swash plate results in a decrease of rotation time and angle of the slipper around its axis. During the rotation of shaft with the swash plate with a constant speed, the slipper also rotates around the piston axis. During each rotation, there are two long periods with the same rotation speed as for the shaft and two very short periods with sudden angular deceleration and acceleration (Figure 17). During reciprocal motion of slipper along the piston axis, the thickness of lubricant between the slipper and the swash plate quickly reaches very small value and stabilizes. Therefore, it can be omitted during further analysis. Only squeezing between the slipper and the piston can be considered, which simplifies the calculations. Friction torque in axial bearing is higher than in journal sliding bearing and varies with the rotation angle. Friction torques in journal bearings vary with the rotation angle and have different courses for two bearings of the compressor. The results from the present study regarding the dynamic parameters of the swash plate–slippers–piston assembly and the results of wear for such an assembly from the article [24] can be used to formulate the novel wear model and determine its parameters for it. This is our research task for the nearest future.

Acknowledgement: K. Siczek has been supported by Polish National Centre of Science (NCN) under Project no. DEC-2012/06/A/ST8/00356.

Conflict of Interests: The authors declare that they have no conflict of interest.

References

[1] www.toyota-industries.com/company/business/automobile/compressor/kind_1/.

[2] Tyczewski, P. 2011 Analysis of Reason of Damage Refrigeration Compressors, Logistyka, vol. 3, pp. 2871-2875.

[3] Gorny K., Tyczewski P., Zwierzycki W. 2010 Characteristics of stands for wear tests of materials for refrigeration compressors elements, Tribologia, vol. 3, pp. 75-84.

[4] Gorny K., Tyczewski P., Zwierzycki W. 2010 The Estimation of the Influence of Mixture Compressor Oils and Refrigerants on the Durability of Nodes of Friction in Cooling Compressors, Tribologia, vol. 4, pp. 117-128.

[5] Latas, W., Stojek, J., Dynamic Model of Axial Piston Swash-Plate Pump for Diagnostics of Wear in Elements, The Archive of Mechanical Engineering, vol. 57, No 2, 2011, 135-155, doi: 10.2478/v10180-011-0010-x.

[6] Chen, H.X., Patrick, S.K. Chua, Lim G.H., Dynamic vibration analysis of a swash-plate type water hydraulic motor. Mechanism and Machine Theory, vol. 41, Issue 5, 2006, pp. 487-504.

[7] Nishimura, T., Umeda, T., Tsuta, T., Fujimara, M., Kamakami, M., Dynamic response analysis of a swash-plate type hydraulic piston pump. ASME, 1995, pp. 145-155.

[8] Vacca, A., Klop, R., Ivantysynova, M., A numerical approach for the evaluation of effects of air release and vapour cavitation on effective flow rate of axial piston machines. International Journal of Fluid Power, No 1, 2010, pp. 33-45.

[9] Latas, W., Stojek, J., Dynamic Model of Axial Piston Swash-Plate Pump for Diagnostics of Wear in Elements, The Archive of Mechanical Engineering, vol. 57, No 2, 2011, 135-155.

[10] Lee, G.H., Lee, T.J., A Study on the Variable Displacement Mechanism of Swash Plate Type Compressor for Automotive Air Conditioning System, 2004, International Compressor Engineering Conference at Purdue, Paper 1706, https://docs.lib.purdue.edu/icec/1706.

[11] Stulgies, N., Gräber, M., Tegethoff, W., Försterling, S., Evaluation of Different Compressor Control Concepts for a Swash Plate Compressor, Proceedings 7th Modelica Conference, Como, Italy, Sep. 20-22, 2009, pp. 299-303.

[12] Changqing Tian, Yunfei Liao, Xianting Li, A mathematical model of variable displacement swash plate compressor for automotive air conditioning system, International Journal of Refrigeration, 2006, vol. 29, issue 2, pp. 270-280.

[13] Zhang, Y., Wang, W., Using overflow in a swash plate compressor for automotive air conditioning system, 2012, Proceedings of the Institution of Mechanical Engineers, Part A: Journal of Power and Energy, vol. 226, issue 4, pp. 564-579.

[14] Mobley, R.K., Fluid Power Dynamics. Chapter 3 Hydraulic Pumps, 2000, pp. 25-46.

[15] Zloto, T., Stryjewski, P., Load of the kinematic pair piston-cylinder block in an axial piston pump, TEKA. Commission of Motorization and Energetics in Agriculture – 2012, Vol. 12, No. 2, 291–296.

[16] Borghi, M., Zardin, B., Specchia, E., Pintore, F., Corradini, E., (2011). Displacement Control In Variable Displacement Axial Piston Swashplate Type Pumps, Proceeding of the Twelfth Scandinavian International Conference on Fluid Power, SICFP'11 Tampere, Finland, Vol. 3.

[17] Kassem, S.A., Bahr, M.K., Effect of Port Plate Silencing Grooves on Performance of Swash Plate Axial Piston Pumps, Current Advances in Mechanical Design and Production VII, Proceedings of the Seventh Cairo University International MDP Conference Cairo-Egypt, February 15–17 2000, pp. 139-148.

[18] Wang, S., Tomovic, M., Liu, H., Commercial Aircraft Hydraulic Systems, Chapter 2 - Aircraft Hydraulic Systems, Shanghai Jiao Tong University Press Aerospace Series, Aerospace Engineering, 2016, pp. 53-114.

[19] Filipi, Z., Alternative Fuels and Advanced Vehicle Technologies for Improved Environmental Performance, Chapter 16 Hydraulic and pneumatic hybrid powertrains for improved fuel economy in vehicles, Chapter 16.3.1 Hydraulic pump/motors, 2014.

[20] Pourmovahed, A., Beachley, N.H., Fronczak, F.J., Modelling of a hydraulic energy regeneration system. Part I. Analytical treatment, Transactions of the ASME: J. Dynamic Systems, Measure-

ment and Control, 114: 155-159 (1992).
[21] Kim, JH., Jeon, CS. & Hong, YS. Constant pressure control of a swash plate type axial piston pump by varying both volumetric displacement and shaft speed, Int. J. Precis. Eng. Manuf. (2015) 16: 2395.
[22] Huang, J., Yan, Z., Quan, L., Lan, Y., & Gao, Y. (2015). Characteristics of delivery pressure in the axial piston pump with combination of variable displacement and variable speed. Proceedings of the Institution of Mechanical Engineers, Part I: Journal of Systems and Control Engineering, 229(7), 599–613.
[23] Srivastava, P., Sharma, K., and Jha, R., Modeling of Fixed Displacement Swash Plate Compressor: A Mathematical Approach towards Calculation of Shaft Torque and Volumetric Efficiency, SAE Technical Paper 2016-28-0172, 2016.
[24] Woźniak M., Batory D., Siczek K., ANALYSIS FOR THE CASE OF DAMAGE TO THE COOLING AGGREGATE IN VEHICLE WITH COLD STORAGE CHAMBER, Journal of KONES Powertrain and Transport, Vol. 25, No. 1 2018, pp. 475-82
[25] Xu, B., Hu, M., Zhang, J-H, Su Q., Characteristics of volumetric losses and efficiency of axial piston pump with respect to displacement conditions, J Zhejiang Univ-Sci A (Appl Phys & Eng) 2016 17(3):186-201.
[26] Flores, P., and Lankarani, H.M., Spatial rigid-multi-body systems with lubricated spherical clearance joints: modeling and simulation, Nonlinear Dynamics 60, 1-2 (2009) 99-114.
[27] Pinkus, O., Sternlicht, S.A.: Theory of Hydrodynamic Lubrication, McGraw Hill, New York, (1961).
[28] Radulescu, A.V., Radulescu, I., Analysis of squeeze film process between non-parallel circular surfaces, 13th International Conference on Tribology, ROTRIB'16, IOP Conf. Series: Materials Science and Engineering 174 (2017) 012038,.
[29] Naffin, R.K., Chang, L., An Analytical Model for the Basic Design Calculations of Journal Bearings, Journal of Tribology, APRIL 2010, Vol. 132 / 024503-3.
[30] https://medias.schaeffler.com/medias/en!hp.tg.cat/tg_hr*ST4_18687224075#ST4_20922158859.
[31] https://www.timken.com/wp-content/uploads/2018/10/Timken-Thrust-Bearing-Catalog_10765.pdf.